RSC Advances

COMMUNICATION

View Article Online
View Journal | View Issue

Cite this: *RSC Adv.*, 2014, **4**, 48017

Structure and stability of two dimensional phosphorene with =O or =NH functionalization†

Jun Dai and Xiao Cheng Zeng*

Received 31st March 2014
Accepted 23rd September 2014

DOI: 10.1039/c4ra02850c

www.rsc.org/advances

We investigate the stability and electronic properties of oxy-(=O) or imine-(=NH) functionalized monolayer phosphorene with either single-side or double-side functionalization based on density-functional theory calculations. Our thermodynamic analysis shows that oxy-functionalized phosphorene can be formed under the conditions ranging from ultrahigh vacuum to high concentrations of molecular O_2, while the imide-functionalized phosphorene can be formed at relatively high concentrations of molecular N_2H_2. In addition, our Born–Oppenheimer molecular dynamics (BOMD) simulation shows that under ambient conditions both O_2 and N_2H_2 can etch phosphorene away.

Recently, a new two-dimensional (2D) semiconductor, phosphorene, has been successfully isolated through mechanical cleavage of crystalline black phosphorus.[1–4] It has been demonstrated that phosphorene-based field-effect transistors (FETs) can exhibit a high on/off ratio ($\sim 10^5$) and relatively high carrier mobility (up to 1000 $cm^2\ V^{-1}\ s^{-1}$),[1,2,4] suggesting potential applications of phosphorene in nano-electronic devices. Black phosphorus, the bulk counterpart of phosphorene, is the most stable form of phosphorus and was discovered by Bridgman in 1914.[5] Like graphite, black phosphorus is also a layered material with weak interlayer van der Waals (vdW) interaction. In each layer, the phosphorus atom is bonded with three adjacent phosphorus atoms, forming a puckered honeycomb structure.[6,7] The three bonds take up all three valance electrons of phosphorus atom. Thus, a monolayer phosphorene is a 2D semiconductor with a direct bandgap of about 0.3 eV.[8–12] More interestingly, the direct bandgap feature of few-layer phosphorene is dependent on the thickness. Previous theoretical calculations show that the bandgap can be tuned from 1.5 eV for monolayer to 0.6 eV for 5-layer phosphorene.[13] Furthermore, either in-plane or out-of-plane strain can significantly change the bandgap of monolayer phosphorene. Indeed, a ~5% in-plane strain can convert the monolayer phosphorene from a direct-gap to an indirect-gap semiconductor,[2] while a vertical compression can induce the semiconductor-to-metal transition.[14] The in-plane anisotropic optical properties of phosphorene[15,16] and its potential applications in solar-cell systems[17] have also been reported.

Although black phosphorus is the most stable allotrope of phosphorus, it is still reactive under ambient condition.[5,18–20] Especially, it has been reported that phosphorene flakes can be etched away at ambient condition.[20] We also note that for graphene, chemical functionalization can be an effective way to tune its electronic properties.[21–29] Therefore, it is useful to study stability and properties of chemical functionalized phosphorene sheets. Note also that carbon and phosphorus have different valence electron configuration, namely, $2s^22p^2$ for carbon and $3s^23p^3$ for phosphorus. In graphene, three valence electrons in carbon form sp^2 orbitals and the remaining valence electrons, one in each carbon atom, form delocalized π orbital. On the other hand, in phosphorene, phosphorus forms sp^3 bonding with a lone pair of valence electrons in each phosphorus atom. Therefore, the chemical species used for chemical functionalization of graphene may not be suitable for functionalization of phosphorene.

Here, we consider divalent electron donors such as =O, =S, =NH and $=CH_2$ for possible phosphorene functionalization in view of successful synthesis of organophosphonates whose simplest forms include $O{=}PH_3$, $S{=}PH_3$, $HN{=}PH_3$ and $H_2C{=}PH_3$.[30,31] The structures and thermodynamic stabilities of these divalent ligands functionalized phosphorene are carefully examined. Effect of the functionalization on the electronic structure of phosphorene is also discussed. We show that oxy-(=O) functionalized phosphorene can be automatically formed in the presence of O_2 with either high or low O_2 concentration, while imide-(=NH) functionalized phosphorene can be automatically form in relatively high concentration of N_2H_2. Our BOMD simulations show that both oxy- and imide-

Department of Chemistry, University of Nebraska-Lincoln, Lincoln, NE 68588, USA. E-mail: xzeng1@unl.edu

† Electronic supplementary information (ESI) available. See DOI: 10.1039/c4ra02850c

functionalization can etch phosphorene away at the ambient condition in the presence of either O_2 or N_2H_2.

For density-functional theory (DFT) calculations, the generalized gradient approximation (GGA) for the exchange-correlation potential is adopted. The plane-wave cutoff energy for wave function is set to 500 eV. The ion-electron interaction is treated with the projected augmented wave (PAW)[32,33] method as implemented in the Vienna *ab initio* simulation package (VASP 5.3).[34,35] For geometry optimization, a 8 × 10 × 1 Monkhorst–Pack *k*-mesh is adopted for functionalized phosphorene systems. A vacuum spacing of ~20 Å is used so that the interaction between adjacent layers can be neglected. During the geometric optimization, both lattice constants and atomic positions are relaxed until the residual force on atoms are less than 0.01 eV $Å^{-1}$ and the total energy change is less than 1.0×10^{-5} eV. In addition, a combination of optB88-vdW[36,37] for geometry optimization and HSE06 (ref. 38) for band structure calculation (based on the optB88-vdW optimized structure) is used, which has been proven very reliable for few-layer phosphorene systems.[2] Our benchmark calculations for bulk black phosphorus also confirm reliability of the selected two DFT methods (see ESI Fig. S1†).

Four divalent adsorbates, namely, =O, =S, =NH and $=CH_2$ are initially considered for functionalization of the phosphorene monolayer. However, our calculations show that S atoms cannot effectively bond to P atoms while $=CH_2$ can disrupt the integrity of phosphorene (see ESI Fig. S2†). Hereafter, we only focus on =O and =NH functionalized phosphorene. Both single-side and double-side functionalization are taken into account. For simplicity, we use **P–O-half** and **P–O** notations to denote single-side and double-side =O functionalized phosphorene, and **P–NH-half** and **P–NH** for the single-side and double side =NH functionalized phosphorene. The optimized structures are shown in Fig. 1 and the structural parameters of **P–O-half**, **P–O**, **P–NH-half**, and **P–NH** are summarized in Table 1. One can see that the functionalization with four different patterns on phosphorene share some common features. Firstly, the functionalization with =O and =NH results in an in-plane structural expansion, where the in-plane lattice constant *a* expands over 4.9–12.5% while *b* expands over 11.7–21.0% with different functionalization patterns. As a result, the in-plane P–P bond length also expands. The P–P bond length that is out of the *xy* plane expands over 1.3–5.6%. These expansions stem from the weakening of bond strength since these adsorbates are electron acceptors which can fetch electrons from P atoms (see ESI Table S1†). Another intriguing feature is that in **P–O-half**, the difference in bond length for two types of P–P bonds is almost negligible.

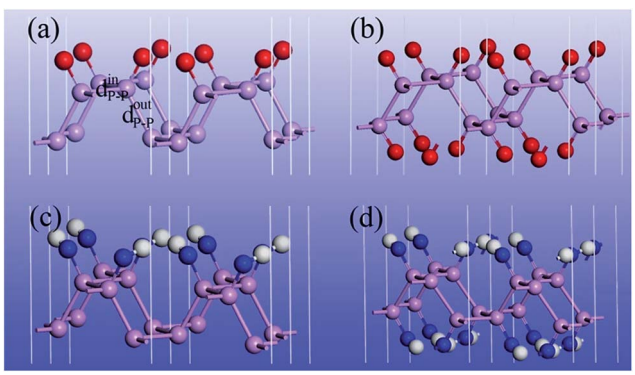

Fig. 1 Optimized structure of (a) **P–O-half**, (b) **P–O**, (c) **P–NH-half** and (d) **P–NH**. Red, white, blue and pink spheres denote oxygen, hydrogen, nitrogen and phosphorus atoms, respectively. d^{in}_{P-P} and d^{out}_{P-P} denotes the P–P bond length in and out of the *xy* plane.

Table 1 Computed optimized geometry parameters, including P–P bond length in the *xy* plane (d^{in}_{P-P}), P–P bond length out of the *xy* plane (d^{out}_{P-P}),. P–X (X=O, N) bond length (d_{P-x}), in-plane lattice constants (*latt. const.*), and adsorption energies for functionalized phosphorene monolayer. **P–O-half**, **P–O**, **P–NH-half**, **P–NH** and **P** denote monolayer phosphorene with single-side =O functionalization, double-side =O functionalization, single-side =NH functionalization, double-side –NH functionalization and pristine monolayer phosphorene, respectively

	d^{in}_{P-P} (Å)	d^{out}_{P-P} (Å)	d_{P-x} (Å)	*latt. const.* (Å)	E_{ad} (eV)
P–O-half	2.283	2.283	1.478	$a = 5.091$, $b = 3.469$	4.132
P–O	2.338	2.380	1.483	$a = 5.514$, $b = 3.690$	4.184
P–NH-half	2.288	2.304	1.555	$a = 5.136$, $b = 3.492$	2.634
P–NH	2.386	2.367	1.562	$a = 5.466$, $b = 3.719$	2.754
P	2.220	2.253	N/A	$a = 4.556$, $b = 3.305$	N/A

Adsorption energies for the functional groups are computed at the HSE06 level, which is defined as: $E_{ad} = -(E_{tot} - E_P - nE_x)/n$, where E_{tot} is the total energy of the functionalized phosphorene with *n*X (X = O or NH) as ligands, E_P is the energy of pristine phosphorene monolayer, and E_x is the energy of an isolated X. According to this definition, a larger value of E_{ad} means stronger adsorption. As shown in Table 1, the average adsorption energy in the double-side functionalization is slightly greater than that in the single-side functionalization. Besides, the adsorption of =O is significantly stronger than that of =NH, because =O is a stronger electron acceptor than =NH. Thus, the **P–O** bonding is stronger than P–N.

Similar to the definitions used in the discussion of the thermodynamic stability of functionalized graphene nanoribbons[39,40] and graphene oxides,[41] we define the zero temperature formation energies of the functionalized phosphorene as:

$$E_f^x = \frac{1}{N}\left(E^{tot} - E_P - \frac{N_x}{2}E_x\right),$$

where E^{tot} and E_P are the total energy of the functionalized phosphorene and the pristine phosphorene, E_x is the energy of the isolated O_2 or N_2H_2 molecule, N_x is the number of O= or =NH in a supercell, and *N* is the number of phosphorus atom in a supercell. The stability of different structures can be determined by E_f^x under different experimental conditions. For example, in the presence of molecular O_2 gas, the relative stability can be obtained by comparing

$$G_{O_2} = E_f^{O_2} - \rho_O\frac{\mu_{O_2}}{2},$$

where $\rho_O = N_O/N$, at the absolute temperature T, and for a partial O_2 pressure P, the chemical potential of O_2 can be obtained as:

$$\mu_{O_2} = H^\circ(T) - H^\circ(0) - TS^\circ(T) + k_B T \ln\frac{P}{P^\circ},$$

where $H^\circ(T)$ and $S^\circ(T)$ are the enthalpy and entropy at the pressure $P^\circ = 1$ bar (taken from the JANAF thermochemical tables).[42] For a given value of μ, the structure with a lower value of G is more stable.

In Fig. 2, G *vs.* μ is plotted for the functionalized phosphorenes. First, we can see that **P–O** is more stable than **P–O-half** for all negative values of the O_2 chemical potential, suggesting that the **P–O** is the more stable specie thermodynamically under experimental conditions ranging from ultrahigh vacuum to atmospheric concentration of molecular O_2. For **P–NH** and **P–NH-half**, we can see that **P–NH-half** is more stable than **P–NH** at relatively low values of N_2H_2 chemical potential, while at relatively high values of N_2H_2 chemical potential, **P–NH** is more stable than **P–NH-half**. Thus, under the experimental condition of ultralow concentration of N_2H_2, **P–NH-half** is more stable, while under the condition of relatively high N_2H_2 concentration, **P–NH** is more stable than **P–NH-half**. Second, Fig. 2 suggests that phosphorene is unstable in the presence of O_2 even in the ultrahigh vacuum concentration of molecular O_2 (G is negative), and oxy-functionalized phosphorene can be automatically formed. In the presence of N_2H_2, phosphorene is unstable under condition of relatively high concentration of N_2H_2, and the imine-functionalized phosphorene can be automatically formed as well. To address the substrate induced lattice change in real systems, we computed the formation energies of **P–O** and **P–NH** with a uniaxial strain of 5% or −5% along a or b axis, or a biaxial strain of 5% or −5% along both a and b. The results are summarized in ESI Table S2.† One can see that a net effect of the strain on the G–μ curves as shown in Fig. 2 is a shift along the y axis in a range of +0.001 to +0.067 eV, therefore, will not change the conclusion regarding the thermal stability of **P–O** and **P–NH**.

We have also studied thermal stability of the functionalized phosphorene by means of the BOMD simulations with the constant-pressure and constant-temperature (NPT) ensemble. Here, the pressure is set to 1 atm, while the temperature is controlled at either 70 K or 300 K. The time step is 2 fs, and the total simulation time is 8 ps. As shown in Fig. 3, at the low temperature (70 K), structures of **P–O-half**, **P–O** and **P–NH-half** are still robust and intact, indicating their stability near liquid nitrogen temperature. But for **P–NH**, the structure is partially destroyed, indicating at relatively high concentration of N_2H_2, phosphorene can be etched away. Near the room temperature (300 K), none of the four functionalized phosphorene sheets can retain their structure integrity, especially for the **P–NH** one which would decompose into several clusters with a huge volume expansion. The BOMD simulations indicate that these functionalized phosphorene sheets can be possibly observed at low temperature in the presence of either O_2 or N_2H_2, while at high temperature, phosphorene can be etched away.

Lastly, we examine effects of the chemical functionalization on the electronic structures of phosphorene monolayer. Our benchmark calculations show that unlike half-hydrogenated or half-fluorinated graphene systems[43,44] for which their magnetic properties can be tuned by surface functionalization, here the four functionalized phosphorene sheets appear to be non-spin-polarized. This is because phosphorus atoms in phosphorene adopt the sp^3 hybridization; the adsorbates act as electron acceptor and bond with P atoms with the electron lone pairs on P atoms. Hence, there are no unpaired electrons and spin polarization in these systems. The HSE06 band structures and atomic projected density of states (pDOS) are plotted in Fig. 4. Except for **P–O**, the direct bandgap feature is not retained in **P–O-half**, **P–NH-half** and **P–NH**. The bandgap of **P–O-half** (1.55 eV) is close to pristine monolayer phosphorene (~1.5 eV).[13] The bandgap in other three functionalized phosphorene sheets are slightly reduced to 1.03 eV, 1.44 eV and 1.24 eV for **P–O**, **P–NH-half** and **P–NH**, respectively. Moreover, in functionalized phosphorene sheets, the VBM is a hybrid state in which O or NH contributes the most part, while the CBM is nearly contributed by P atoms. It is worthy of mentioning that although previous theoretical calculations have shown that the ~5% in-plane compression can convert monolayer phosphorene from being a direct-gap to an indirect-gap semiconductor,[2] the studied

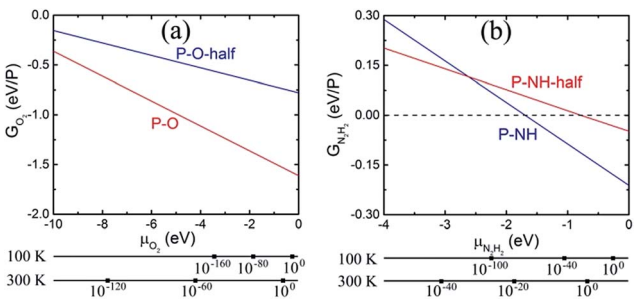

Fig. 2 Formation energies *versus* chemical potential for (a) **P–O-half** and **P–O**, (b) **P–NH-half** and **P–NH**. The alternative axes show the pressure, in bar, of molecular O_2 and N_2H_2 gases corresponding to the chemical potential at $T = 100$ K and 300 K.

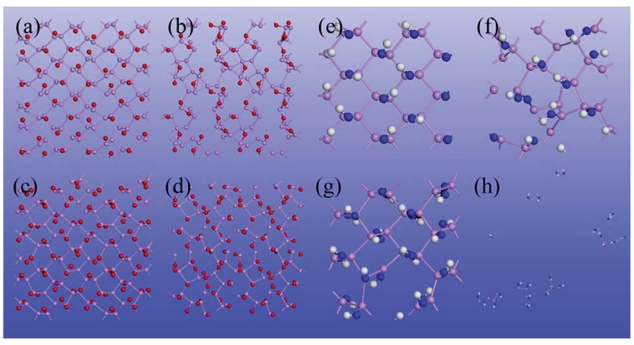

Fig. 3 Snapshots of functionalized phosphorene monolayer at 8 ps of the Born–Oppenheimer molecular dynamics simulation in the NPT ensemble, (a) **P–O-half** at 70 K, (b) **P–O-half** at 300 K, (c) **P–O** at 70 K, (d) **P–O** at 300 K, (e) **P–NH-half** at 70 K, (f) **P–NH-half** at 300 K, (g) **P–NH** at 70 K and (h) **P–NH** at 300 K.

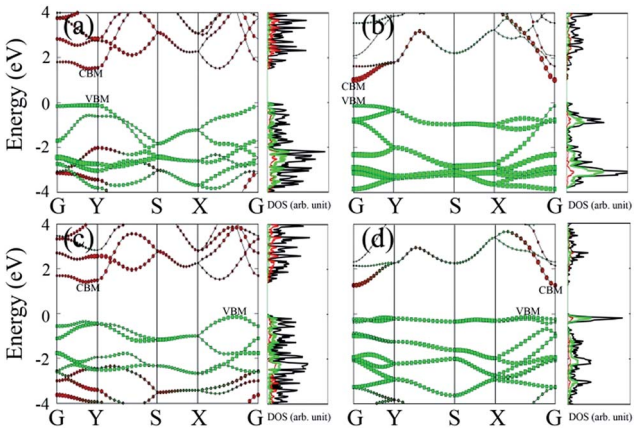

Fig. 4 HSE06 band structure and atomic projected partial density of states (pDOS) of (a) P–O-half, (b) P–O, (c) P–NH-half and (d) P–NH. The Fermi level is set to 0. In band structures, the size of red spheres and green rectangles (lines) denote the contribution from P and O (or NH), and valence band maximum and conduction band minimum and labelled as VBM and CBM, while in pDOS, black, red and green lines denote the total DOS, pDOS of P and O (or NH), respectively.

phosphorene-based FET devices still have relatively good properties. Possible contamination of phosphorene by O_2 or N_2H_2, especially O_2, should also be carefully monitored since the contamination can harm performance of the devices.

Conclusions

We investigate properties of oxy-(=O) and imine-(=NH) functionalized monolayer phosphorene with either single-side or double-side functionalization. Our thermodynamic analysis shows that in the presence of molecular O_2 with either high or low concentration, oxy-functionalized phosphorene will be automatically formed while imide-functionalized phosphorene will be formed at relatively high concentration of N_2H_2. Moreover, our BOMD simulation suggests that at ambient conditions the phosphorene will be etched away.

Notes and references

1 L. Li, Y. Yu, G. J. Ye, Q. Ge, X. Ou, H. Wu, D. Feng, X. H. Chen and Y. Zhang, *Nat. Nanotechnol.*, 2014, **9**, 372–377.
2 H. Liu, A. T. Neal, Z. Zhu, Z. Luo, X. Xu, D. Tománek and P. D. Ye, *ACS Nano*, 2014, **8**, 4033–4041.
3 E. S. Reich, *Nature*, 2014, **506**, 19.
4 F. Xia, H. Wang and Y. Jia, *Nat. Commun.*, 2014, **5**, 4458.
5 P. Bridgman, *J. Am. Chem. Soc.*, 1914, **36**, 1344–1363.
6 J. C. Jamieson, *Science*, 1963, **139**, 1291–1292.
7 A. Brown and S. Rundqvist, *Acta Crystallogr.*, 1965, **19**, 684–685.
8 R. W. Keyes, *Phys. Rev.*, 1953, **92**, 580.
9 H. Asahina and A. Morita, *J. Phys. C: Solid State Phys.*, 1984, **17**, 1839.
10 T. Takahashi, H. Tokailin, S. Suzuki, T. Sagawa and I. Shirotani, *J. Phys. C: Solid State Phys.*, 1985, **18**, 825.
11 D. Warschauer, *J. Appl. Phys.*, 2004, **34**, 1853–1860.
12 H. Guo, N. Lu, J. Dai, X. Wu and X. C. Zeng, *J. Phys. Chem. C*, 2014, **118**, 14051–14059.
13 J. Qiao, X. Kong, Z.-X. Hu, F. Yang and W. Ji, *Nat. Commun.*, 2014, **5**, 4475.
14 A. Rodin, A. Carvalho and A. Neto, *Phys. Rev. Lett.*, 2014, **112**, 176801.
15 R. Fei and L. Yang, *Nano Lett.*, 2014, **14**, 2884.
16 V. Tran, R. Soklaski, Y. Liang and L. Yang, *Phys. Rev. B: Condens. Matter Mater. Phys.*, 2014, **89**, 235319.
17 J. Dai and X. C. Zeng, *J. Phys. Chem. Lett.*, 2014, **5**, 1289–1293.
18 T. Nishii, Y. Maruyama, T. Inabe and I. Shirotani, *Synth. Met.*, 1987, **18**, 559–564.
19 S. P. Koenig, R. A. Doganov, H. Schmidt, A. Neto and B. Oezyilmaz, *Appl. Phys. Lett.*, 2014, **104**, 103106.
20 A. Castellanos-Gomez, L. Vicarelli, E. Prada, J. O. Island, K. Narasimha-Acharya, S. I. Blanter, D. J. Groenendijk, M. Buscema, G. A. Steele and J. Alvarez, *2D Materials*, 2014, **1**, 025001.
21 S. Ryu, M. Y. Han, J. Maultzsch, T. F. Heinz, P. Kim, M. L. Steigerwald and L. E. Brus, *Nano Lett.*, 2008, **8**, 4597–4602.
22 D. Elias, R. Nair, T. Mohiuddin, S. Morozov, P. Blake, M. Halsall, A. Ferrari, D. Boukhvalov, M. Katsnelson and A. Geim, *Science*, 2009, **323**, 610–613.
23 J.-A. Yan, L. Xian and M. Chou, *Phys. Rev. Lett.*, 2009, **103**, 086802.
24 J. T. Robinson, J. S. Burgess, C. E. Junkermeier, S. C. Badescu, T. L. Reinecke, F. K. Perkins, M. K. Zalalutdniov, J. W. Baldwin, J. C. Culbertson and P. E. Sheehan, *Nano Lett.*, 2010, **10**, 3001–3005.
25 M. A. Ribas, A. K. Singh, P. B. Sorokin and B. I. Yakobson, *Nano Res.*, 2011, **4**, 143–152.
26 F. Withers, T. H. Bointon, M. Dubois, S. Russo and M. F. Craciun, *Nano Lett.*, 2011, **11**, 3912–3916.
27 V. Georgakilas, M. Otyepka, A. B. Bourlinos, V. Chandra, N. Kim, K. C. Kemp, P. Hobza, R. Zboril and K. S. Kim, *Chem. Rev.*, 2012, **112**, 6156–6214.
28 M. Z. Hossain, J. E. Johns, K. H. Bevan, H. J. Karmel, Y. T. Liang, S. Yoshimoto, K. Mukai, T. Koitaya, J. Yoshinobu and M. Kawai, *Nat. Chem.*, 2012, **4**, 305–309.
29 J. Dai, Y. Zhao, X. Wu, X. C. Zeng and J. Yang, *J. Phys. Chem. C*, 2013, **117**, 22156–22161.
30 N. A. Hosea, H. A. Berman and P. Taylor, *Biochemistry*, 1995, **34**, 11528–11536.
31 I. Alkorta, G. Sánchez-Sanz, J. Elguero and J. E. Del Bene, *J. Phys. Chem. A*, 2014, **118**, 1527–1537.
32 P. E. Blöchl, *Phys. Rev. B: Condens. Matter Mater. Phys.*, 1994, **50**, 17953.
33 G. Kresse and D. Joubert, *Phys. Rev. B: Condens. Matter Mater. Phys.*, 1999, **59**, 1758.
34 G. Kresse and J. Furthmüller, *Phys. Rev. B: Condens. Matter Mater. Phys.*, 1996, **54**, 11169.
35 G. Kresse and J. Furthmüller, *Comput. Mater. Sci.*, 1996, **6**, 15–50.
36 M. Dion, H. Rydberg, E. Schröder, D. C. Langreth and B. I. Lundqvist, *Phys. Rev. Lett.*, 2004, **92**, 246401.

37 J. Klimeš, D. R. Bowler and A. Michaelides, *Phys. Rev. B: Condens. Matter Mater. Phys.*, 2011, **83**, 195131.
38 J. Heyd, G. E. Scuseria and M. Ernzerhof, *J. Chem. Phys.*, 2006, **124**, 219906.
39 T. Wassmann, A. P. Seitsonen, A. M. Saitta, M. Lazzeri and F. Mauri, *Phys. Rev. Lett.*, 2008, **101**, 096402.
40 A. P. Seitsonen, A. M. Saitta, T. Wassmann, M. Lazzeri and F. Mauri, *Phys. Rev. B: Condens. Matter Mater. Phys.*, 2010, **82**, 115425.
41 L. Wang, Y. Sun, K. Lee, D. West, Z. Chen, J. Zhao and S. Zhang, *Phys. Rev. B: Condens. Matter Mater. Phys.*, 2010, **82**, 161406.
42 M. W. Chase Jr, C. A. Davis, J. R. Downey Jr, D. J. Fruip, R. A. McDonald, and A. N. Syverud, JANAF Thermochemical Tables, *Journal of Physical and Chemical Reference Data*, 3rd ed, 1985.
43 J. Zhou, Q. Wang, Q. Sun, X. Chen, Y. Kawazoe and P. Jena, *Nano Lett.*, 2009, **9**, 3867–3870.
44 J. Zhou, M. M. Wu, X. Zhou and Q. Sun, *Appl. Phys. Lett.*, 2009, **95**, 103108.